# Multi-objective topology optimization of deep drawing dissimilar tailor laser welded blanks; experimental and finite element investigation

**Aminzadeh, A., Parvizi, A. & Moradi, M.**



**Original citation & hyperlink:**
Aminzadeh, A, Parvizi, A & Moradi, M 2020, 'Multi-objective topology optimization of deep drawing dissimilar tailor laser welded blanks; experimental and finite element investigation', Optics and Laser Technology, vol. 125, 106029. https://dx.doi.org/10.1016/j.optlastec.2019.106029

DOI 10.1016/j.optlastec.2019.106029
ISSN 0030-3992

Publisher: Elsevier

# Multi-Objective Topology Optimization of Deep Drawing Dissimilar Tailor Laser Welded Blanks; Experimental and Finite Element Investigation

Ahmad Aminzadeh[1], Ali Parvizi[2] Mahmoud Moradi[3, 4*]

1- School of Mechanical Engineering, College of Engineering, University of Tehran, Tehran, Iran

E-mail: aminzadeh.a@ut.ac.ir

2- Assistant Professor, School of Mechanical Engineering, College of Engineering, University of Tehran, Tehran, Iran

E-mail: aliparvizi@ut.ac.ir, Tel: +98 21 61119953

3- Department of Mechanical Engineering, Faculty of Engineering, Malayer University, Malayer, Iran

4- Laser Materials Processing Research Center, Malayer University, Malayer, Iran

*Corresponding author: E-mail: moradi.malayeru@gmail.com

**Abstract**

Laser welded blanks (LWBs) are semi-finished components typically manufacture by dissimilar materials, thicknesses, shapes, coatings, etc. After butt welding of the primary sheets, the product sheets are subjected to the sheet metal forming process. Formation of the heat-affected zones (HAZ) is typical in LWBs, which possess quite different mechanical properties than the base materials. Recently, laser beam technologies have been widely employed to weld different types of vehicles panels. In this study applying Nd:YAG laser welding, experimental and numerical investigations are carried out to evaluate the effects of process input factors on deep drawing process of LWBs. Laser beam power, welding speed, blank holder force (BHF), material properties, and friction coefficient are considered as process key input parameters. In addition, the laser welding and deep drawing processes were numerically simulated using Simufact Welding and Abaqus/Explicit software, Used the Simorgh supercomputer for heavy modeling calculations. Moreover, drawing depth, weld line movement, and energy absorption are taken into account as process main outputs or objective functions. Besides, using an advanced MATLAB code, multi objective optimization based on genetic algorithm is applied to determine the optimal design input parameters. It is observed that the critical stresses were taken place outside the weld zone and rupture due to high heat input of laser and metallurgical changes of the base metal occur in the pre-softening zone. In addition, the weld line displacement occurs as a result of plastic strain change of the weld joint that causes failure-prone zone creation as well as the adverse wrinkling. By considering weld line displacement and absorbed energy as multi-objective function, the optimal points is 1.15 mm and 0.21 KJ for weld line displacement and absorbed energy, respectively. Good agreement between the simulated and the experimental results revealed that the model would be appropriate for deep drawing of LWB process numerical simulation.

***Keywords***: Laser welded blanks (LWBs); Deep drawing; FEM; Multi-objective optimization; weld line movement; Finite Element Method.

| **Nomenclature** | |
|---|---|
| *LWBs* | Laser welded blanks |
| *HAZ* | heat affected zones |
| *BHF* | blank holder force |
| *TWB* | Tailor welded blank |
| TTT | time-temperature-transformation |
| *LFT* | lotus root filled tube |
| *ANN* | artificial neural network |
| *DOE* | design of experiment |
| *RSM* | response surface method |
| *TR* | transition region |

## 1. Introduction

In several industries, the requirement for cost-effective products and lightweight with excellent performance is essential for success. Tailor welded blank (TWB) structures have been widely used in automobile, aerospace and transportation. Because of the significant increasing request for dissimilar strengths in construction, Applying Tailored Welded Blank (TWB) sheets is one of the solutions to manufacture light-weighted vehicles. Consequently, researchers have investigated the formability of TWBs by considering different methods based on experimental and simulation studies. The preliminary investigations were conducted to explore different advantages of TWBs such as cost reduction, reduced weight, and increased strength. Furthermore, this process ensures that the finished part features the right material in the right place. These sheets are welded according to various materials, thicknesses, shapes, coatings, and sizes. Then, they typically subjected to forming processes at a specific temperature to accomplish the desired shape. Different

welding processes such as laser, TIG, GTAW, resistance spot, and friction stir have been applied in manufacturing of TWBs. In between, laser welding offers some outstanding advantages such as low distortion, high process speed, and low general heat input that make it more attractive for numerous product lines, especially in the automotive industry [1–4]. Nowadays, Laser Welded Blanks (LWBs) are used to manufacture automobile components such as side frames, pillars, rails, and panels, which are thin near the lock and thick near the hinges to withstand different types of corrosions or loads. LWBs which are generally made of steel, aluminum, and other dissimilar materials are lighter and often cheaper than the conventional sheets [5] .In this regard, integrating the controlling process parameters may decrease total cost rate and increase process performance or optimize both of them.

Considering different aspects of TWBs, performing experimental work to investigate mechanical properties and validation by finite elements method for analysis of several parameters affecting the quality of the laser welded joints [6,7]. Rojek et al. [8] reported diverse techniques to determine the mechanical properties of the weld zone in TWBs. Nd:YAG Laser sources are broadly used for engineering applications such as cutting, drilling and welding [9]. Liu et al.[10] measured simultaneously of the welding temperature and clamping force for a butt welded joint during Nd:YAG laser welding. The results shown that there is an optimal clamping force improves the weld joint strength. Yilbas et al. [11] analyzed thermal stress in term of theoretical and experimental laser welding of low carbon steel. It is found that after the solidification of the molten regions von Mises stress attains at high values. Pulse Nd:YAG laser beam welding parameters such as laser beam power, spot diameter and have a lot of effects on penetration as well as microstructure characterization in different types of material and thicknesses [12,13]. Wang et al. [14]evaluated three types of laser beam oscillating welding on aluminum alloy sheets. Among

them, the best weld quality in terms of reducing the porosity in the weld and increasing the tensile strength was the infinity mode. Assunção et al. [15] conducted a comparative experimental and numerical studies at the automotive industry to compare steel LWBs fabricated by three different types of high-power lasers such as $CO_2$, Nd:YAG with different heat inputs, and fiber laser in terms of productivity, costs, and weld quality. Based on experiment study the impacts of various shielding gas and flow rates of $CO_2$ laser of dissimilar materials (DP600/TRIP700 steel) on local mechanical properties investigated. They reported that higher helium shielding gas along with better flow rate result in deeper weld penetration and lower weld width [16,17]. Safari et al. [18] carried out a new experimental and FE model irradiating scheme for laser bending of tailor machined blanks has been proposed. In another study, Safari et al.[19] designed a novel method for laser forming of two-step bending of a dome shaped part with a continuous $CO_2$ laser welding machine. In addition they [20] carried out laser forming of a saddle shape with spiral irradiating scheme. Based on the results, the curvatures of obtained saddle shape are increased considerably by increasing the number of irradiation passes,

Weld line displacement is one of the defects in forming of TWBs sheets. Numerous researches have been conducted to study this item. investigate of different factors such as punch and die radii, thickness ratio, selective heating, friction coefficient, and blank holder force (BHF) are critical parameters in weld line movement [21,22]. Deep drawing of high strength TWBs with design and manufacturing special tailored dies made by two different materials improve the forming behavior in sheet metal forming operations [23–25]. According to the experimental and FEM method as well as using Infrared Thermography (IR) and Digital Image Correlation (DIC), the lower ductility of the base metal together with competition between two failure mechanisms, delamination and namely metal failure. [26,27]. Considering the influences of eight main process parameters, the

deep drawing process was investigated by Kardan et al. [28] To evaluate the process outputs comprising punch force and sheet thickness variation through experimental study. Moreover, they [29] conducted the experimental and simulation investigations to minimize the residual stress in cylindrical deep drawing process. Padmanabhan et al. [30] conducted several numerical simulations to determine the stress states and the influences on the spring back behavior of deep-drawn tailor welded blanks. Safdarian et al. [31] carried out experimental and theoretical investigation of effect of thickness ratio (TR) on the formability and forming limit diagram (FLD) of St12 steel sheets during laser welded blanks. Results shown that formability and the level of FLD will decrease by raising the difference of thickness ratio of LWB and LTR. Rahmatabadi et al.[32–34] conducted several experimental evaluation of tensile fracture surfaces, micro hardness test, mechanical properties, crystallite size of samples and optical microscope and FLD of different multi-layered composite strips. Safari and Joudaki [35] investigated deformation of a pre-punched sheet due to the roll forming with respect to bow defect and ovality.

In a recent study, Multi-objective crashworthiness and lightweight optimization for the side construction of an automobile body was performed by Xiong et al.[36]. They used the IPM method identifies the optimal result from the achieved Pareto set. Moreover, design of vehicle parts under impact loading and multi-objective optimization for weight minimization as well as maximum energy absorption were established. Rahmatabadi et al. [37] evaluated of rupture energy absorption capacity and fracture toughness of as rolled LZ71 and LZ91 Mg alloy sheet in term of automobile applications. Guangyong et al.[38] Investigation of Multi-objective optimization of a vehicle door using multiple material tailor-welded blank (TWB) technology. However, they demonstrated that the proposed method is suitable for multi-material topology optimization (MMTO) and the multi-objective of TWB indoor panel. Furthermore, Safari, and Joudaki [39] predated bending angle of

tailor machined blanks in laser forming process by neural network. They show neural network with 5×8×1 trained be able to forecast the bending angle with acceptable accuracy. A novel system based on artificial neural network (ANN) model was developed by Dhumal et al. [40] to predict the deep drawing behavior of TWBs made of steel grade base materials. Based on a multi-objective genetic algorithm regression models, Hamidinejad et al. [41] investigated the laser beam welding (LBW) technology of (IF) galvanized steel sheets of interstitial free (IF) used in the automobile industrial. Reisgen et al. [42] conducted numerical and RSM optimization technique in $CO_2$ laser beam welding. They found that, when the experimenter does not have a model for the process RSM could be considered as a powerful tool in experimental welding optimization.

To the best of authors knowledge, there is no study which investigates the multi-objective optimization of the simultaneous effects of five key process parameters including welding speed, laser power, blank holder force (BHF), material properties, and friction coefficient in deep drawing process of LWBs. Furthermore, the deep drawing process was carried out along with controlling the input parameters to minimize the weld line displacement as well as to maximize the drawin depth and energy absorption. The adequate number of experiments are defined based on design of experiment (DOE). Using the Simufact welding and Abaqus software, the welding and forming processes are wholly simulated considering the thermal-mechanical coupling analysis. The model was verified through comparing the results with the experimental outputs. Moreover, the proposed model is optimized by multi-objective optimization based on genetic algorithm to find the optimum outputs as well as determine the influence of each input parameter. The scattered distribution and Pareto frontier diagram are drawn to define the optimal solution for better overview of the optimized design factors and the objective functions.

## 2. Material and experiments

St14, St44, and TPP Low carbon steel plates with thickness of 1mm were considered as sheets to be utilized in welding process. The chemical composition of the material is presented in Table 1.

**Table 1.** Chemical composition of base materials

| Materials | S | P | Mn | Si | N | C | Al |
|---|---|---|---|---|---|---|---|
| **St14** | - | - | - | - | - | 0.08 | 0.2 |
| **St44** | 0.04 | 0.04 | 1.6 | 0.55 | 0.009 | 0.21 | - |
| **TPP** | - | - | - | - | 0.07 | 0.1 | - |

As mentioned before, these materials (low carbon steel) were taken from Simufact welding comprehensive material database have a relatively high coefficient of specific heat capacity and thermal expansion, as seen in Fig. 1, (a) and (b) [43].

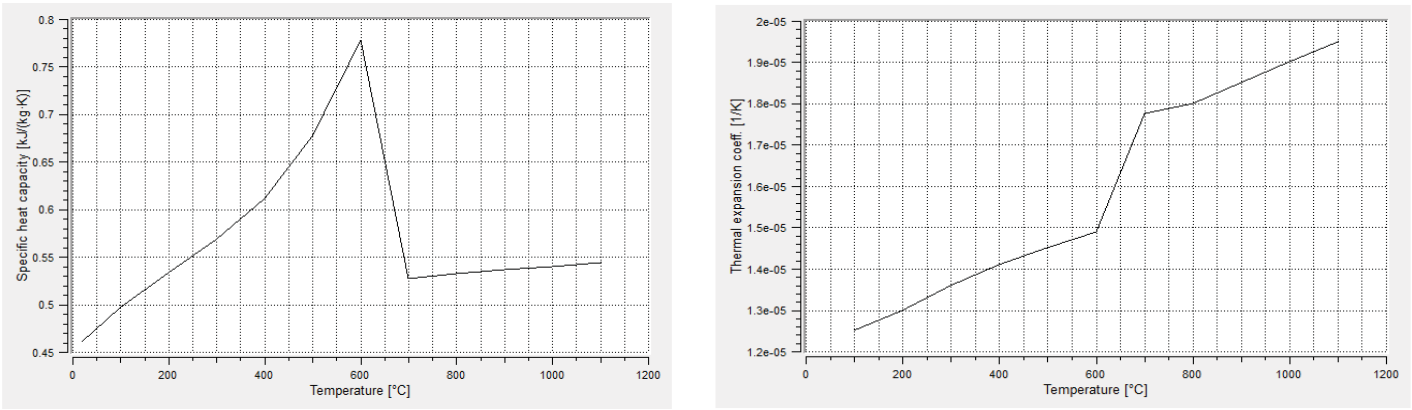


(a) (b)

**Fig. 1**. Material properties (a) specific heat capacity (b) thermal expansion

To define the material properties and preparing the blanks for experiments, samples and tensile specimens were cut using four-axial CNC punching machine at Irankhodro Automotive Industry as illustrated in Fig. 1. In order to determine the anisotropic characteristics of the sheet, the tensile

test specimens were cut out with 1 mm thickness at three different directions, i.e. 0, 45, and 90 degree based on ASTM E8M-04 [44] as shown in Fig. 2 (b). The measured data of mechanical properties are given in Table 2.

Five key process factors including coefficient of friction between die components, blank holder force (BHF), welding speed, laser power, and material types are considered as input parameters. Besides, weld line displacement, drawing depth, and absorbing energy are taken into account as process outputs. The process factors and the associated levels are given in Table 3 in which four factors with continuous values and one categorical parameter are considered.

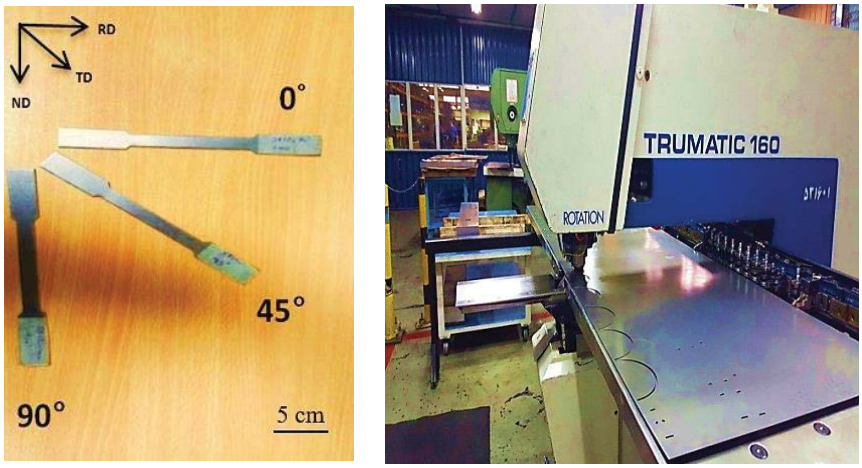


(a) (b)

**Fig. 2.** (a) Tensile test specimens (b) Cutting process with CNC milling machine

**Table 2**. Mechanical properties of St 14, St 44 and TPP sheets

| | St 14 | | | St 44 | | | TPP | | |
|---|---|---|---|---|---|---|---|---|---|
| **Degree** | **0** | **45** | **90** | **0** | **45** | **90** | **0** | **45** | **90** |
| **Yield stress (MPa)** | 230 | 240 | 180 | 280 | 300 | 285 | 270 | 285 | 270 |
| **Ultimate stress (MPa)** | 350 | 420 | 410 | 350 | 500 | 520 | 520 | 500 | 520 |
| **Young's modulus (GPa)** | | 210 | | | 210 | | | 210 | |
| **Density (kg/m$^3$)** | | 7800 | | | 7800 | | | 7800 | |
| **Poisson's ratio** | | 0.3 | | | 0.3 | | | 0.3 | |

**Table 3.** Levels of process parameters in welding and deep drawing process

| Factor | Name | Units | Type | Low Actual | High Actual |
|---|---|---|---|---|---|
| A | Blank holder force (BHF) | N | Numerical | $5\times10^4$ | $1.5\times10^5$ |
| B | Friction coefficient | - | Numerical | 0.1 | 0.2 |
| C | Welding speed | mm/s | Numerical | 7.4 | 10.75 |
| D | Laser power | W | Numerical | 100 | 300 |
| E | Material | - | Categorical | St14-St44 | TPP-St44 |

Based on Design Expert software recommendation, 35 experiments with D-optimal system was investigated. These experiments that designed based on response surface method (RSM) are demonstrated in Table 4. For all experiments, a quantity of each factor level could be achieved from data given in Table 3.

Initially, the joining surfaces were cleaned by acetone and subsequently polished to avoid any contaminations for achieve better welding quality. Then, sheets were welded using A pulsed Nd:YAG laser (IQL-10 model) with a maximum average power of 400W was used to make bead on plate welds. A set of Rotameter flow meters was used to measure the shielding gas flow rate. The coaxial shielding gas nozzle with a 5 mm diameter was positioned at 2 mm distance from the work-piece surface. $CO_2$ and $O_2$ gases were added to argon gas. In order to avoid inadvertent welding condition (such as too much spatter or porosity), an initial series of experiments were performed and the following parameters were found to give reasonably sound welds and shapes making it possible to focus on the effect of shielding gas composition on weld profile. The available range for the laser parameters were: pulse energy at 11 J, pulse duration at 7 ms, pulse frequency 20 Hz, travel speed 7.4 mm/s, and shielding gas flow rate 60 lit/min. The focal length

of focusing optical system was 75 mm giving a laser spot size of about 800 μ at above the work piece. Laser welding process as shown in Fig. 3. Fig. 4 depicts all of the experimental specimens utilized in laser welding process. Specimens subjected to NDT inspection test and three samples were rejected.

**Table 4.** D-optimal designed array for experiments

| | | Forming settings | | Laser Welding settings | | |
|---|---|---|---|---|---|---|
| **Experiment No.** | **Run order** | **Blank holder force (BHF)(N)** | **Friction** | **Welding Speed(mm/s)** | **Laser Power(W)** | **Materials** |
| 1 | 2 | 50000 | 0.2 | 10.75 | 100 | St14-St44 |
| 2 | 9 | 97062 | 0.13 | 10.75 | 300 | TPP-St14 |
| 3 | 13 | 150000 | 0.2 | 7.4 | 300 | TPP-St44 |
| 4 | 5 | 50000 | 0.1 | 7.4 | 100 | St14-St44 |
| 5 | 4 | 50000 | 0.2 | 7.4 | 300 | TPP-St14 |
| 6 | 31 | 50000 | 0.1 | 10.75 | 100 | TPP-St44 |
| 7 | 18 | 124191 | 0.1 | 10.28 | 100 | St14-St44 |
| 8 | 16 | 98595 | 0.1 | 7.4 | 100 | TPP-St14 |
| 9 | 29 | 150000 | 0.1 | 10.75 | 300 | TPP-St44 |
| 10 | 1 | 150000 | 0.2 | 7.4 | 100 | St14-St44 |
| 11 | 33 | 150000 | 0.1 | 10.75 | 100 | TPP-St14 |
| 12 | 28 | 50000 | 0.2 | 7.4 | 100 | TPP-St44 |
| 13 | 7 | 81667 | 0.16 | 7.4 | 206.82 | St14-St44 |
| 14 | 22 | 150000 | 0.2 | 10.75 | 224.92 | TPP-St14 |
| 15 | 34 | 50000 | 0.1 | 7.4 | 300 | TPP-St44 |
| 16 | 19 | 50000 | 0.1 | 10.75 | 300 | St14-St44 |
| 17 | 21 | 50000 | 0.2 | 10.75 | 100 | TPP-St14 |
| 18 | 12 | 150000 | 0.1 | 7.4 | 100 | TPP-St44 |
| 19 | 26 | 89250 | 0.2 | 8.85 | 300 | St14-St44 |
| 20 | 6 | 150000 | 0.16 | 8.64 | 100 | TPP-St14 |
| 21 | 23 | 50000 | 0.2 | 10.75 | 300 | TPP-St44 |
| 22 | 32 | 150000 | 0.1 | 7.4 | 300 | St14-St44 |
| 23 | 10 | 50000 | 0.1 | 9.14 | 210.68 | TPP-St14 |
| 24 | 8 | 150000 | 0.2 | 10.75 | 100 | TPP-St44 |
| 25 | 24 | 150000 | 0.17 | 10.75 | 300 | St14-St44 |
| 26 | 30 | 80274 | 0.15 | 10.33 | 189.89 | St14-St44 |
| 27 | 20 | 75000 | 0.17 | 8.68 | 137.97 | TPP-St14 |
| 28 | 25 | 112500 | 0.11 | 8.88 | 209.81 | TPP-St44 |
| 29 | 35 | 119065 | 0.1 | 7.45 | 180.06 | St14-St44 |
| 30 | 15 | 80468 | 0.2 | 10.38 | 225 | TPP-St14 |

| | | | | | | |
|---|---|---|---|---|---|---|
| 31 | 17 | 150000 | 0.2 | 10.75 | 100 | TPP-St44 |
| 32 | 14 | 150000 | 0.2 | 7.4 | 300 | TPP-St44 |
| 33 | 11 | 97062 | 0.13 | 10.75 | 300 | TPP-St14 |
| 34 | 3 | 50000 | 0.1 | 10.75 | 100 | TPP-St44 |
| 35 | 27 | 50000 | 0.1 | 10.75 | 300 | St14-St44 |

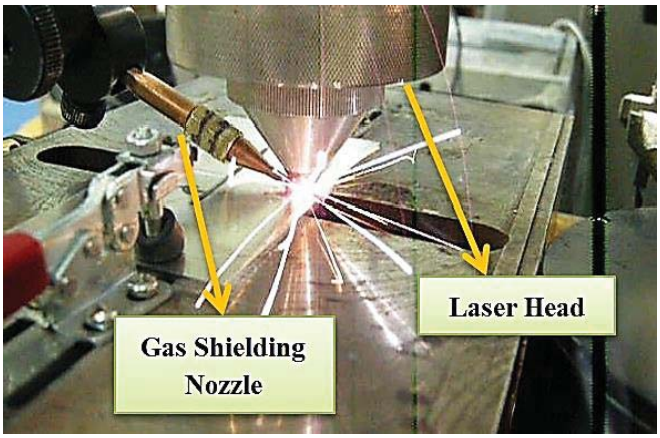


**Fig 3.** Nd:YAG Laser welding Process

Deep drawing of LWBs made of low carbon steel was performed using a 315 tons hydraulic Müller press. According to the Fig 5 and Fig 6, a special die was designed based on Table 5 and manufactured at Irankhodro automotive Industry. The punch and die matrix material was selected from VCN200 steel to avoid heat treatment, as well as good abrasion resistance against drawing tests. The ram speed and blank holder force (BHF) were adjusted at continues levels using control valve of the hydraulic machine.


**Fig 4.** LWBs with Nd:YAG laser process

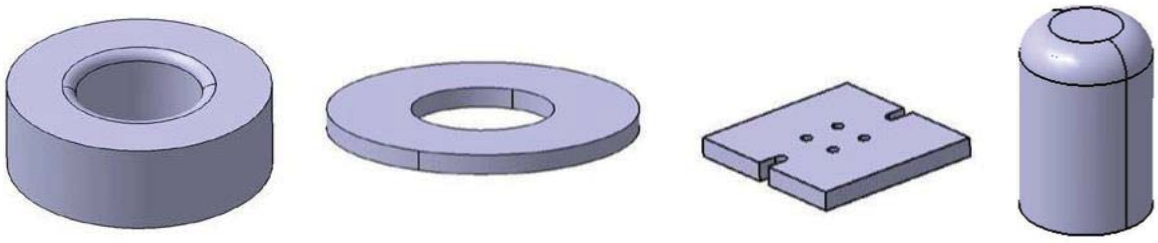

(a) (b) (c) (d)

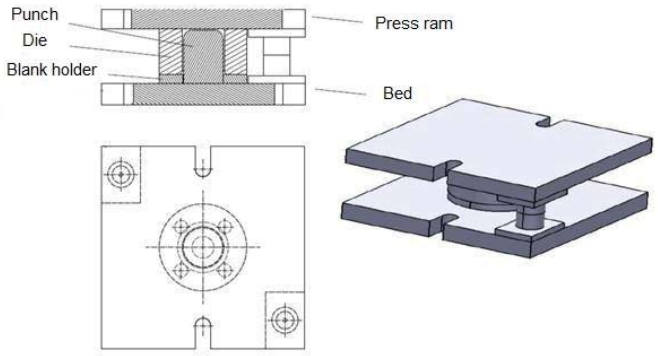


(e)

**Fig 5**. CAD design of deep drawing Die a) Die b) Blank holder c) Press ram d) Punch e) Assembly parts

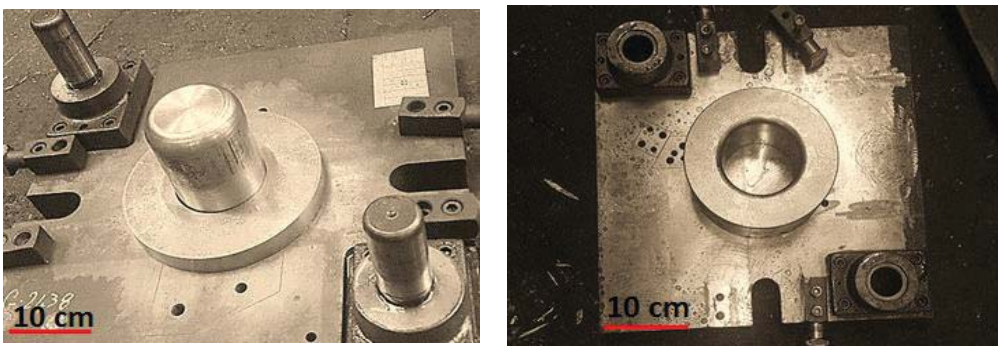


**Fig 6.** Die configuration for deep drawing process

**Table 5.** Dimension of die components

| Die components | Dimension (mm) |
|---|---|
| Punch diameter | 90 |
| Pound edge radius | 20 |
| Punch height | 123 |
| Blank holder outer diameter | 200 |
| Blank holder inner diameter | 92 |
| Die outer diameter | 200 |
| Die inner diameter | 100 |
| Die edge radius | 10 |
| Die height | 105 |

## 3. Finite element simulation

The numerical simulations were divided in two parts welding and forming. The deep drawing simulations were conducted using FEM tool Abaqus/Explicit, whereas the welding simulations with Simufact welding 6.0 from MSC Software. The thermal and mechanical temperature-dependent material properties used in the model are shown in Fig. 1 and are given from the material

library software. In laser simulation, welding process was adjusted at 200 seconds. In addition, thermo-mechanical coupling was considered in simulation. Fig. 7 shows the weld line motion and clamping set up during laser welding is shown. Main equations, initial and boundary conditions used in the simulation work are based on same study of laser simulation [45]. The hexahedral elements, DCAX4, were designed for the thermal analysis. In addition, trial and error method has been carried out through the simulation for define mesh sensitivity. Welding sequence, initial conditions and structural welding simulation was designed based on Simufact welding software library. Initial condition as follow:

- Using finite element mesh information on discretized geometry provided.
- Using comprehensive material database for thermomechanical and Thermophysical properties.
- Information on heat sources including welding sequence and welding velocity
- Fixture structure and condition

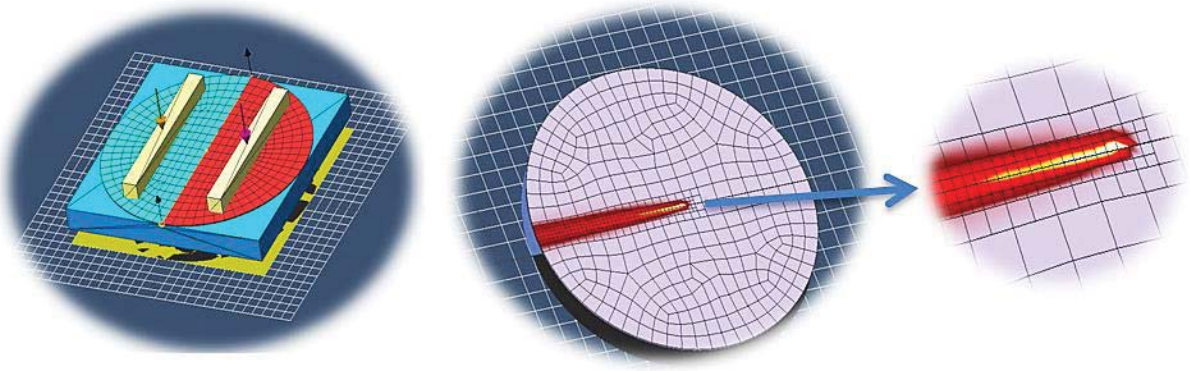

**Fig 6.** Simulation of welding process in Simufact Welding

During the simulation, multi-phase composition and temperature characteristics based on Simufact welding library were applied. Depending on the amount of heat supplied, the maximum

temperatures (306 – 1450 °C) change. In addition, the cooling dynamics in the temperature range of 700 – 200 °C.

Taking completed the welding simulation, all properties of the weld model were exported from Simufact Welding to Abaqus software to simulate the deep drawing process. The Simorgh supercomputer (AMD 48-core v 48 gig memory per node) was used for heavy modeling calculations. Also, Eight-node brick element with reduced integration, C3D8R was applied. Number of element in the base metal and weld zone are 4,194 and 20,000, respectively. Sample 3 of experiment, as defined in Table 4, was chosen to be simulated by FE model. Outcomes of FE model containing drawing depth and displacement of the weld line were compared with experimental samples to validate the developed model. In addition, the friction coefficient between the surfaces was measured by sliding friction tests. To define the friction behavior between the die components coulomb friction model was used. This procedure was applied to all sets of test designed based on RSM, according to Table 2. The axisymmetric model of cup is demonstrates in Fig. 7.

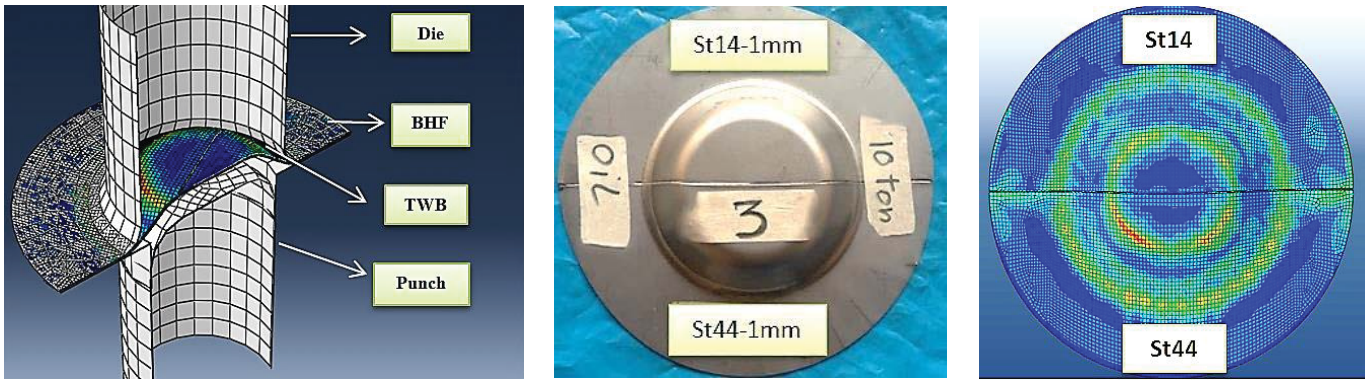


(a) (b) (c)

**Fig 7**. FE model of deep drawing LWBs in ABAQUS software (a) die components (b) experimental sample (c) FE model

Low carbon steel was considered as sheet material in FE simulation. Elastic and plastic properties of St 44 carbon steel in three directions, i.e. 0, 45 and 90 degrees, were assigned accordance of equations defined in ABAQUS user's manual. According to equation 2, in materials science, a general rule of mixtures (ROM) is a method of approach to the approximate estimation of the composition of material properties. Consequently, rule of mixture is adapted to describe the material behavior at the weld line [46]. The material properties of the weld line in various combinations of LWBs are calculated as follows and the results are presented in Table 6.

$$X_{w=}(0.55)X_{BM1} + (0.45)X_{BM2} \quad (2)$$

Where suffixes $X_{BM1,}$ $X_{BM2}$ and $X_{w}$ stands for mechanical properties in the base metal 1 base metal 2 and weld zone material.

**Table 6.** Material properties of weld line applied in the simulation

| Materials | Young's Modulus (GPa) | Ultimate Stress (MPa) | Yield Stress (MPa) |
|---|---|---|---|
| **St14-St44** | 210 | 456 | 267 |
| **St14-TPP** | 210 | 456 | 260.25 |
| **TPP-St44** | 210 | 500 | 291.75 |

## 4. Results and discussion

### 4.1. Metallurgical investigation

One of the most challenges in laser welding process is a huge effects of thermal and cooling rate in the welding region and various microstructure as well as specific hardness profile. Thus, measurement of the hardness has a key role in the laser welding operation. There are elastic and dynamic processes to measure hardness. Here, hardness measurements were done at ten different

points based on ISO 6508 standard. Fig. 8 presents the specimen as well as the measurement process.

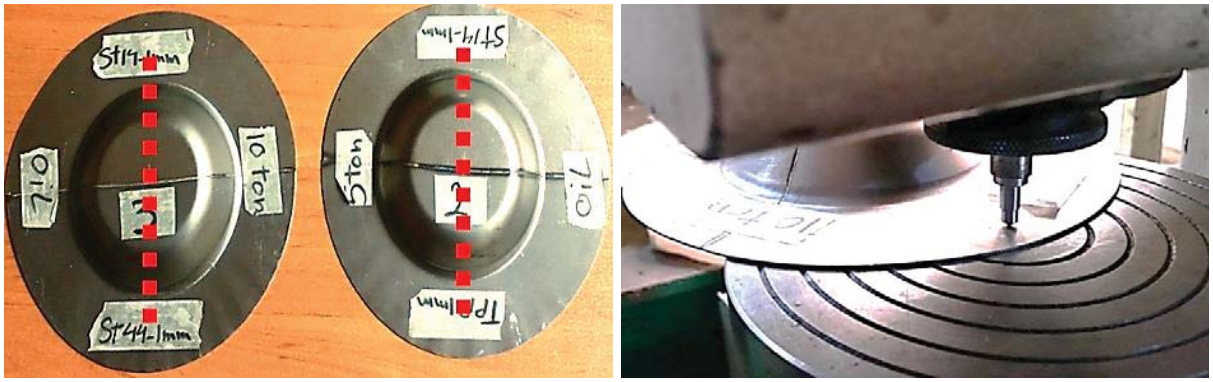


(a) (b)

**Fig 8**. (a) Specimen for hardness measurements (b) hardness measurement process

Based on the thermal processes condition like Nd:YAG laser welding, it is noticeable to pinpoint that the local heat concentration in the joint region of the sheets as well as the quick cooling of the molten material change to the brittle phases. This brittle phase possesses higher values of hardness. The experimental results from the hardness test based on the distance from the welding line are demonstrated in Fig. 9 (a). The hardness value at the intersection area is equal to 345 HB which is significantly high for this type of steel. A remarkable point in this diagram is the softening zone or the hardness valley located in the area affected by external heat. The measurements indicate that the hardness values at HAZ are even lower than the as-received metals which are almost 119.8 and 116.2 HB for St44 and St14 steels, respectively.

The SEM image of microstructure at the welded joint is shown in Fig. 9 (b). According to Fig. 9 (b), crack is not observed at the transition region (TR) of sample. However, there are some voids at TR which are not big enough to be critical. According to literature [46], the maximum softening rate of the HAZ occurred in the area where phase transformation resulted in domination of Peritectoid pearlite phase, i.e. soft phase. Regarding the reduction of the softening area, it can be

argued that the rate of softening reduces as the welding speed increases. In the same line, the width and drawing depth of the softening area reduce with increasing the welding speed. This is also being affected by the level of heat input. Generally, rupture is taken place in the pre-softening or failure zone.

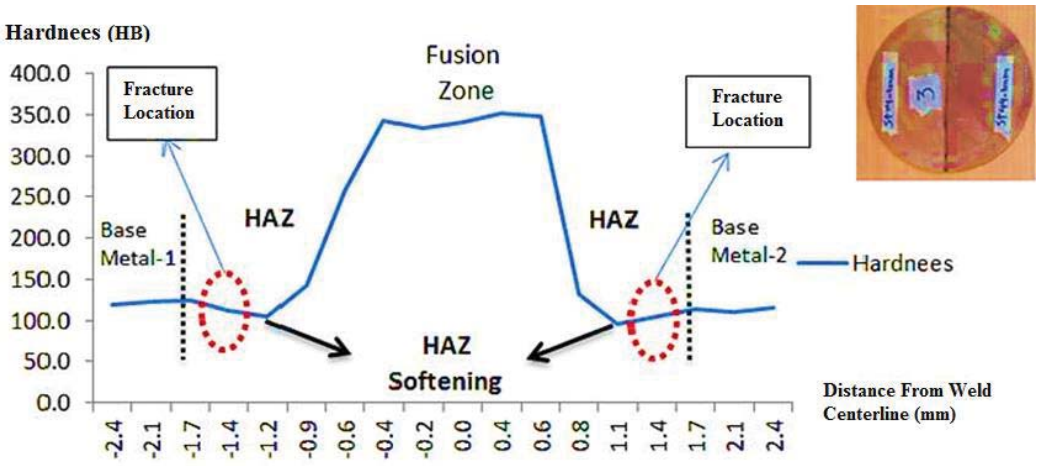


(a)

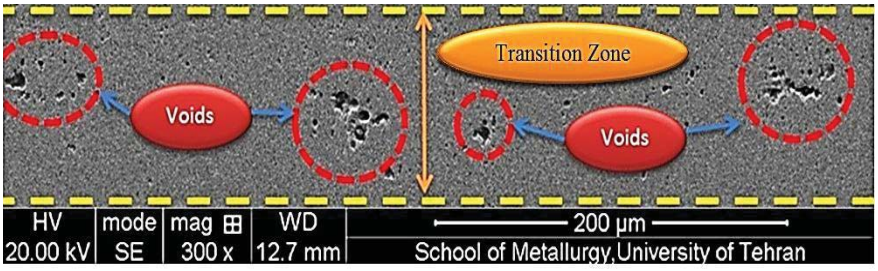


(b)

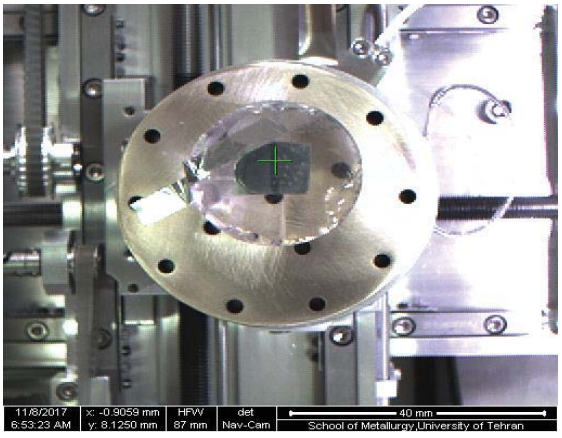


(c)

**Fig. 9**. Metallurgical investigation of laser welding sample # 3 (a) Hardness measurement of laser welding process (b, c) SEM micrograph of welded zone

### 4.2 Experimental analysis of laser welding

The present study is carried out using Nd:YAG laser-welding machine and input factors for each sample were adjusted based on in Table 7. It is worth noting that samples with poor welding quality, as well as poor weld bonding and penetration, were excluded from the study to ensure the statistical adequacy of the results. By doing so, the results indicate an acceptable weld diffusion quality.

According to Table 7, the comparison between Sample 1 and Sample 2 indicates a change only in the laser spot size. The deep drawing process (Fig. 10) showed that the welding quality (Sample 2) and rupture strength of the welding zone improved with greater laser spot size. However, an excessive increase in this parameter enhanced the likelihood of brittle fracture, reduced the toughness, and consequently expedited the fracture.

**Table 7**. Nd: YAG laser welding parameters for different Materials.

| **Materials** | **Sample** | **Welding Speed** (mm/s) | **Frequency** (HZ) | **Pulse width** (ms) | **Laser Power** (W) | **Spot Size** (μ) |
|---|---|---|---|---|---|---|
| St14-TPP | 1 | 7.4 | 20 | 7 | 200 | 600 |
| | 2 | 7.4 | 20 | 7 | 200 | 800 |
| St14-St44 | 3 | 7.4 | 20 | 7 | 200 | 800 |
| | 4 | 10.75 | 20 | 7 | 200 | 800 |
| St44-TPP | 5 | 7.4 | 20 | 7 | 200 | 800 |

The comparison between Sample 3 and Sample 4 (Fig. 10) suggests that welding quality and drawing depth both increased when increasing welding speed from 7.4 to 10.75 mm/s in Sample 4. It should be noted that the degree of welding line displacement increases with increased drawing depth. Also, an excessive increase in this parameter will result in flange area wrinkling. As a result, increasing the welding speed is effective in the deep drawing of TWB sheets only when a predefined strategy is adopted to control welding line displacement.

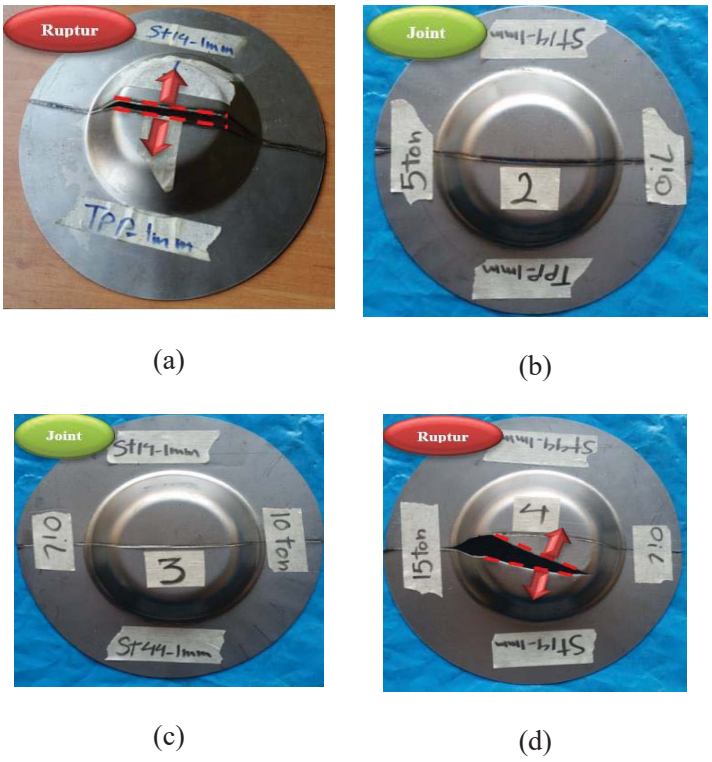


(a) (b)

(c) (d)

**Fig 10**. Comparison between laser welded samples a) Sample 1: Spot size 600 µ, b) Sample 2: Spot size 800 µ c) Sample 3: Welding speed=7.4mm/s d) Sample 4: Welding speed=10.75mm/s

In Sample 4, welding quality and drawing depth both increased when increasing welding speed from 7.4 to 10.75 mm/s. Interestingly, weld line displacement increases with increased drawing depth. Also, an excessive increase in this parameter will result in flange area wrinkling. As a result, increasing the welding speed is effective in the deep drawing of TWB sheets only when a predefined strategy is adopted to control welding line displacement. In sample 5, although the

drawing depth significantly increased, another failure took place in the welding region (Fig. 11). Consequently, there is an optimum condition for improving the depth and failure modes in this case. The measurement of other parameters, such as weld line displacement, does not necessarily produce logical and accurate results.


**Fig 11**. Failure in Sample 5

Table 8 presents the parameters for the deep drawing of LWBs sheets using different materials subjected to laser welding. As it can be seen in Sample 4, the selected blank holder force was greater than the permitted level, resulting in the onset of rupture from the HAZ area and its spread in the metal sheet with lower yield strength. However, in sample 3, the welding speed and quality were higher compared to Sample 4, and the onset of rupture was postponed. Thus, best drawing parameters and the suitable weld penetration was done to Sample 3. As it can be seen in sample 2, no wrinkling was observed on the sheet surface, although the blank holder force was minimal. As a result, in respect to the wrinkling in this case, the best performance was achieved. As previously mentioned, due to inadequate penetration of the molten metal, other laser welding samples did not fulfill the deep drawing criteria and were thus excluded in the data analysis stage.

**Table 8**. Parameters of deep drawing of TWBs sheets of different materials subjected to laser welding

| Sample | Materials | Lubricant | BHF (Ton) | Drawing depth (mm) |
|---|---|---|---|---|
| 2 | TPP-ST14 | Oil-FOX | 5 | 19.4 |
| 3 | ST14-ST44 | Oil-FOX | 10 | 21.2 |
| 4 | ST14-ST44 | Oil-FOX | 15 | 23.5 |

### 4.3. Weld line displacement

One of the most important issues in forming of LWB is weld line displacement after deep drawing process that happens as a result of dissimilar properties of the welded. In addition, weld line displacement from its centerline has a direct effect on the ductility of the sheet. Weld line displacement occurs as a result of plastic strain change of the weld joint that causes to the occurrence of failure-prone zone as well as the adverse wrinkling. It is worth noting that some important parameters such as yield strength, thickness, and sheet geometries have great impact on weld line displacement. In this study, the weld line movement was measured by sketch tracer module of CATIA software. According to Table 9, selecting suitable welding factors including welding speed, the compressive residual stresses caused by welding lead to a higher weld line displacement and drawing depth. Based one sample 2, Weld line displacement is higher than sample 3, i.e. 3.33 mm, due to lower Blank holder force (BHF). Also, in sample 3 weld line displacement is lower than the other cases. It is happened as a result of interaction between bending and hoop stresses during deep drawing process as well as in the sample 4 increase in welding speed compared to sample 3 resulted into higher drawing depth and weld line displacement.

**Table 9**. Results and analysis for weld line displacement

| Materials | Weld line displacement | Deep drawn part |
|---|---|---|
| 2: ST14-TPP | 4.052 mm | 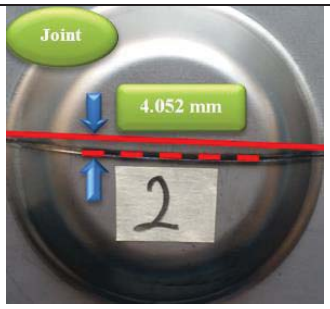  |
| 3:ST14-ST44 | 3.33 mm |   |
| 4:ST44-ST14 | 12.61 mm | 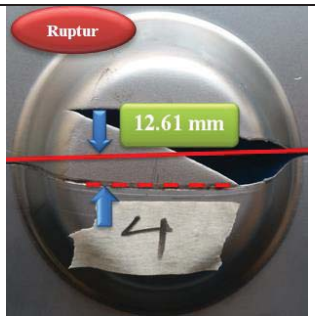  |

### 4.4. Simulation Results

Considering the numerical solution, the developed finite element model was first validated using the experimental results in case of drawing depth and weld line displacement. It should be noted that the punch speed of 33 mm/s and friction coefficient of 0.2 were considered in the simulation. Fig. 13 shows sheets made of two different materials, i.e. St14-TPP. The blank holder force (BHF)

in this set up was 10 tons and the deep drawing was conducted dry for validation test. In this regard, experimental and numerical simulation of drawing depth were 20.2 mm and 18.77 mm, respectively. Based on Figs. 12, the rupture is generally occurred at the specific zone where the combination of welding residual stress and forming stress reach the ultimate stress. Therefore, the crack starts to develop towards the center of the sample. As it can be seen, there is good agreement between the simulated and the experimental results revealed that the model would be appropriate for deep drawing of LWB process numerical simulation.

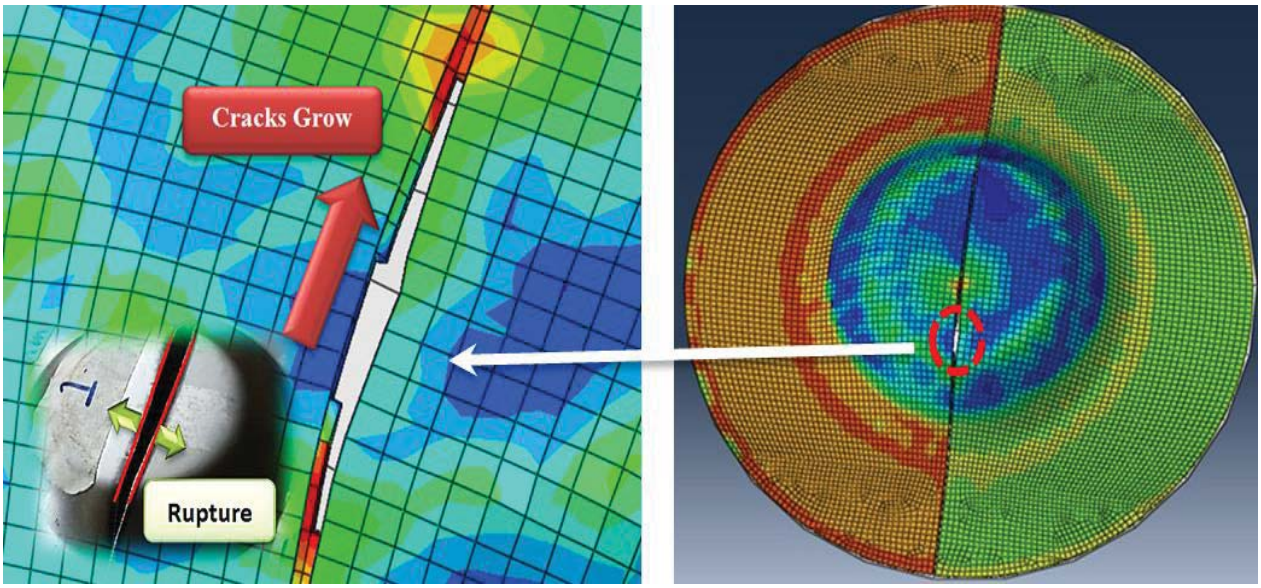


**Fig 12**. Experimental and FE simulation results for rupture and crack growth

Fig. 13 represents the weld line displacement in numerical and experimental cases. According to this figure, the weld line moves towards the stronger metal, i.e. St44. Again, the agreement between the results approves the accuracy of the developed model. Taking validated the FE model, all 35 tests were simulated and the results are demonstrated in Table 10.

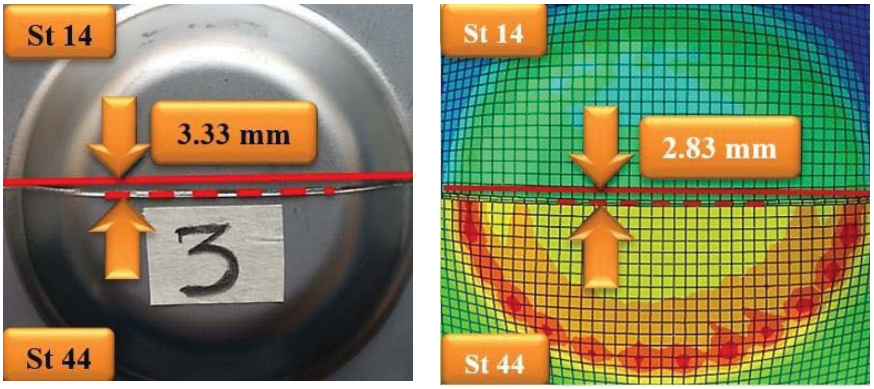


(a) (b)

**Fig. 13**. Comparison of weld line displacement measured by numerical and experimental methods

(a) Experimental sample (b) FE model

**Table 10**. Input and output parameters resulted from FE simulations

| | Input parameters | | | | | Output parameters | | |
|---|---|---|---|---|---|---|---|---|
| **Run** | **Blank holder force (BHF) (N)** | **Friction** | **Welding speed (mm/s)** | **Laser power (W)** | **Materials** | **Drawing depth (mm)** | **Weld displacement (mm)** | **Energy Absorption (KJ)** |
| 1 | 150000 | 0.2 | 7.4 | 100 | st14-st44 | 18.77 | 1.149 | 0.35 |
| 2 | 50000 | 0.2 | 10.75 | 100 | st14-st44 | 22.31 | 2.084 | 0.41 |
| 3 | 50000 | 0.1 | 10.75 | 100 | tpp-st44 | 19.09 | 1.457 | 0.37 |
| 4 | 50000 | 0.2 | 7.4 | 300 | tpp-st14 | 20.66 | 1.054 | 0.37 |
| 5 | 50000 | 0.1 | 7.4 | 100 | st14-st44 | 21.3 | 1.053 | 0.4 |
| 6 | 150000 | 0.16 | 8.64 | 100 | tpp-st14 | 21.81 | 0.861 | 0.47 |
| 7 | 81666.78 | 0.15 | 7.4 | 206.82 | st14-st44 | 23.23 | 2.951 | 0.45 |
| 8 | 150000 | 0.2 | 10.75 | 100 | tpp-st44 | 22.89 | 1.92 | 0.37 |
| 9 | 97061.98 | 0.13 | 10.75 | 300 | tpp-st14 | 22.82 | 1.915 | 0.43 |
| 10 | 50000 | 0.1 | 9.14 | 210.68 | tpp-st14 | 19.75 | 2.146 | 0.44 |
| 11 | 97061.98 | 0.13 | 10.75 | 300 | tpp-st14 | 23.02 | 2.175 | 0.44 |
| 12 | 150000 | 0.1 | 7.4 | 100 | tpp-st44 | 21.21 | 3.365 | 0.42 |
| 13 | 150000 | 0.2 | 7.4 | 300 | tpp-st44 | 21.71 | 3.81 | 0.48 |
| 14 | 150000 | 0.2 | 7.4 | 300 | tpp-st44 | 22.29 | 2.142 | 0.45 |
| 15 | 80468.28 | 0.19 | 10.38 | 225 | tpp-st14 | 22.3 | 1.623 | 0.47 |
| 16 | 98595.47 | 0.1 | 7.4 | 100 | tpp-st14 | 18.69 | 1.676 | 0.36 |
| 17 | 150000 | 0.2 | 10.75 | 100 | tpp-st44 | 21.21 | 2.047 | 0.38 |
| 18 | 124191.3 | 0.1 | 10.28 | 100 | st14-st44 | 22.85 | 1.324 | 0.44 |
| 19 | 50000 | 0.1 | 10.75 | 300 | st14-st44 | 22.27 | 0.983 | 0.44 |

| | | | | | | | | |
|---|---|---|---|---|---|---|---|---|
| 20 | 75000 | 0.17 | 8.68 | 137.97 | tpp-st14 | 19.26 | 2.046 | 0.46 |
| 21 | 50000 | 0.2 | 10.75 | 100 | tpp-st14 | 21.11 | 1.426 | 0.41 |
| 22 | 150000 | 0.2 | 10.75 | 224.917 | tpp-st14 | 22.69 | 2.042 | 0.42 |
| 23 | 50000 | 0.2 | 10.75 | 300 | tpp-st44 | 18.18 | 1.267 | 0.33 |
| 24 | 150000 | 0.17 | 10.75 | 300 | st14-st44 | 19.06 | 2.237 | 0.41 |
| 25 | 112500 | 0.11 | 8.88 | 209.81 | tpp-st44 | 20.62 | 2.12 | 0.47 |
| 26 | 89249.59 | 0.2 | 8.85 | 300 | st14-st44 | 22.18 | 1.458 | 0.5 |
| 27 | 50000 | 0.1 | 10.75 | 300 | st14-st44 | 21.97 | 4.688 | 0.55 |
| 28 | 50000 | 0.2 | 7.4 | 100 | tpp-st44 | 22.52 | 2.643 | 0.41 |
| 29 | 150000 | 0.1 | 10.75 | 300 | tpp-st44 | 18.58 | 1.373 | 0.27 |
| 30 | 80274.19 | 0.14 | 10.33 | 189.89 | st14-st44 | 21.13 | 2.219 | 0.35 |
| 31 | 50000 | 0.1 | 10.75 | 100 | tpp-st44 | 19.09 | 1.811 | 0.33 |
| 32 | 150000 | 0.1 | 7.4 | 300 | st14-st44 | 19.12 | 2.119 | 0.37 |
| 33 | 150000 | 0.1 | 10.75 | 100 | tpp-st14 | 22.31 | 1.768 | 0.42 |
| 34 | 50000 | 0.1 | 7.4 | 300 | tpp-st44 | 20.66 | 1.653 | 0.47 |
| 35 | 119064.7 | 0.10 | 7.45 | 180.1 | st14-st44 | 18.72 | 3.26 | 0.32 |

## 5. Multi-objective optimization

In multi-objective optimization problems especially genetic algorithm, we are dealing with some inconsistent objective functions where outcome the best optimal solutions are problematic. Using Genetic Algorithm (GA) by MATLAB software is a great approach to generate a well-converged diagram solution entitled Pareto frontier [47]. Pareto frontier contains of a set of best value, which reveal both multi-objective solutions and single. In this process, both quality and numerically aspects are determined.

### 5.1 The result of multi-objective optimization

In this study, Multi-objective optimization by changing major factors via an advanced GA is applied to define the optimal value of objective functions. The practical bound of the design factors are listed in Table 11.

**Table 11**. Domain of major decision parameters.

| Design Parameter | Blank holder force (BHF) (N) | Friction | Welding speed (mm/s) | Laser power (W) |
|---|---|---|---|---|
| Lower bound | $5\times10^4$ | 0.1 | 7.4 | 100 |
| Upper bound | $15\times10^4$ | 0.2 | 10.75 | 300 |

According to the Fig. 14, the Pareto frontier graph can be achieved after applying the GA optimization method. This diagram exposes the scattering of the optimal level of both objective functions. Based on Fig. 14, the absorbed energy and weld line displacement vary from 0.325 KJ to 0.51 KJ and 1.15 mm to 2.65 mm, respectively. When weld line displacement is the sole objective function Point A was achieved on Pareto curve whereas point C is when the total absorbed energy is the singular objective function. On the Pareto curve, all the points are the optimal final points and the final choice is based on the policy makers. Nevertheless, in the point D (a theoretical point on the curve), ideal point, both objectives are at their optimal level. Furthermore, this point does not exist on the Pareto cure. Thus, the optimal condition is the neighboring points that have better optimal values compared to other points. Hence, point B is one of the best solutions to this multi-objective problem. It should be noted that every point on the Pareto curve in Fig. 14 has their exclusive design.

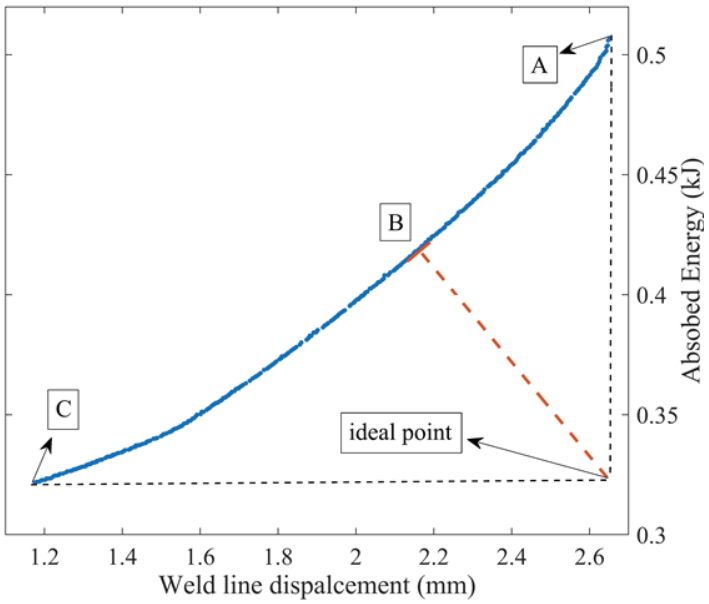


**Fig. 14**. The Pareto frontier optimal distribution for weld line displacement and absorbed energy

The corresponding design values for points A, B and C on the Pareto curve is presented in Table 12. Also, the scattered distribution of design parameters is shown in Fig. 15 to have a great overview of the impact of selected major parameters on the process performance

**Table 12**. The value of multi-objective optimization results.

| Point | Blank holder force (BHF) | Friction | Welding speed (mm/s) | Laser power (W) | weld line displacement (mm) | absorbed energy (KJ) |
|---|---|---|---|---|---|---|
| A | 61273 | 0.1162 | 7.47 | 298.49 | 2.652 | 0.5068 |
| B | 54580 | 0.1009 | 9.23 | 294.72 | 2.157 | 0.4182 |
| C | 97691 | 0.1018 | 10.73 | 122.89 | 1.18 | 0.322 |

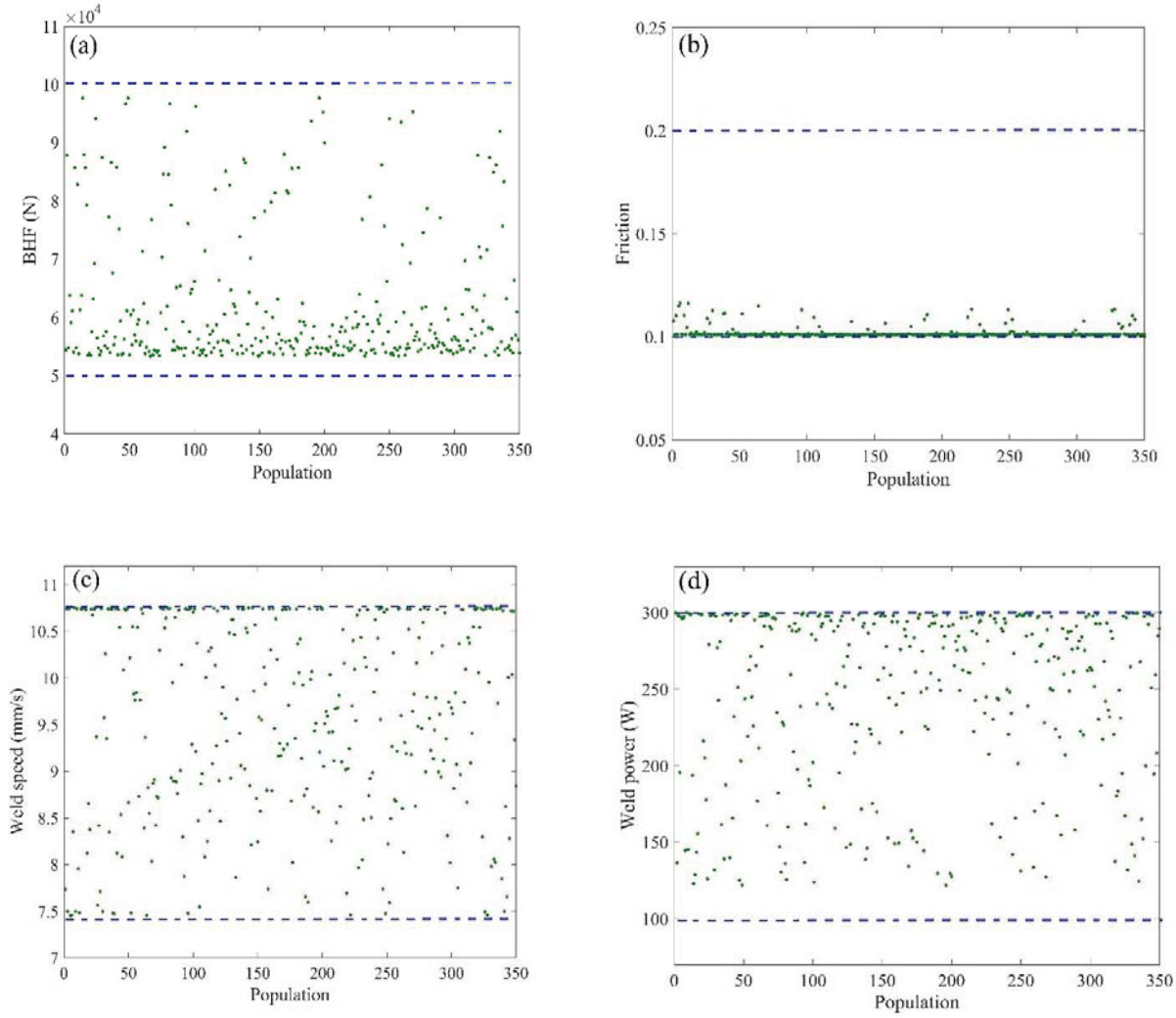


**Fig. 15**. Scattered distribution of the major parameters.

a) BHF-Population b) Friction-Population c) Weld speed-Population d) weld power-Population

Fig. 15(a) shows the distribution of blank holder force (BHF); the figure shows all the optimal points are between $5\times10^4$ < blank holder force (BHF) < $10\times10^4$ N. in order to improve system performance can be select $5.4\times10^4$ N, Because maximum of the optimal points are close to this value. Although several factors play a vital role in the wrinkling like die cavity depth, and radius production, clearances between the blank and die component as well as friction, in this condition,

wrinkling adjust in the minimum level and the material flow has a good distribution. Actually, to prevent the wrinkling and tearing blank holder force can be applied Variable blank holder pressure or hydraulically with pressure feedback. Fig.15 (b) shown the distribution of Friction coefficient in the deep drawing of LWS. In the deep drawing process some factors like drawability of sheet, tool life, and surface quality of finished product are well dependent on presence of good lubricating film between contact surfaces. In this regard, in metal forming processes friction impacts on the drawability of metal sheet and strain distribution [48]. According to the Fig. 15(b), distribution of Friction coefficient between 0.1– 0.2, any value upper than 0.12 is not an appropriate select since there is not any optimal point in this range. As the most of them are close to 0.1 so keeping to better performance. As earlier mention, the process of LWB forming is divided to two section, forming parameters and laser parameters. In this study, in order to achieve the balance between forming and laser welding, this research investigated two factors in each process, which are the most important impact on the formability of LWB. In this regard, with respect to the laser welding, welding speed and welding power are the most essential parameters. Fig. 15(c) shows the distribution of welding speed, it can be determined that since the optimal points cover all ranges of 7.4–10.55 mm/s, this parameter is not sensitive. As it can be seen, with increasing the welding speed to near 10.55 mm/s the welding quality will improve. Furthermore, this result is validated in the experimental analysis. However, this parameter has an optimum condition because in the high level of welding speed the rupture risking in the HAZ zone will increase. As the same condition, based on Fig. 15(d) all the optimal points are near the value of 300 W.

## 6. Conclusion

Considering the input parameters, the deep drawing of TWBs was investigated to minimize the weld line displacement as well as maximize the drawing depth and energy absorption. The number

of experiments was carried out based on design of experiment (DOE). The results for hardness test of softening zone, located in the area affected by outside heat, are incredible. Actually, the measurements indicate that the hardness values at this area are even lower than the as-received metals which are almost 119.8 and 116.2 HB for St44 and St14 steels, respectively. Investigation shows that in case of St14-St44, the interaction between bending and hoop stresses during deep drawing process results into 3.33 mm of weld line displacement. Also, increasing the welding speed results into higher drawing depth and weld line displacement. Moreover, the weld line moves towards the stronger metal, i.e. St44. Taking completed the welding simulation, all properties of the weld model were exported from Simufact Welding to Abaqus software to simulate the deep drawing process. It was shown that the effects of key input process parameters including laser power, welding speed, blank holder force (BHF), and friction coefficient on deep drawing of LWBs are investigated. Additionally, genetic algorithm is used to form the Pareto frontier diagram, which is a set of optimal solution points to evaluate both multi-objective and single optimization results. By considering weld line displacement and absorbed energy as multi-objective function, the optimal value is 1.15 mm and 0.21 KJ for absorbed energy, respectively.

**Acknowledgements**

The authors would like to thank Mr. Amir Mohammad Behzadi for contribution to the optimization analysis.

**References**

[1] M. Moradi, M. Ghoreishi, J. Frostevarg, A.F.H. Kaplan, An investigation on stability of laser hybrid arc welding, Opt. Lasers Eng. 51 (2013) 481–487.

[2] M. Moradi, N. Salimi, M. Ghoreishi, H. Abdollahi, M. Shamsborhan, J. Frostevarg, T. Ilar, A.F.H. Kaplan, M. Moradi, mass balance Parameter dependencies in laser hybrid arc welding by design of experiments and by a mass balance, 022004 (2014). doi:10.2351/1.4866675.

[3] A. Hosein, M. Moradi, M. Goodarzi, P. Colucci, C. Maletta, technology for AA2198 Al-Li alloy, 96 (2017) 1–6.

[4] H. Technology, L. Materials, Effect of Linear Heat Input on the Morphology and Mechanical Properties of Ti-6Al-4V Welded Using a CO 2 Laser, 40 (2018) 49–64.

[5] B. Kinsey, X. Wu, Tailor welded blanks for advanced manufacturing, Elsevier, 2011.

[6] A.A. Zadpoor, J. Sinke, R. Benedictus, Mechanics of tailor welded blanks: an overview, in: Key Eng. Mater., 2007: pp. 373–382. doi:https://doi.org/10.4028/www.scientific.net/KEM.344.373.

[7] S.K. Panda, M.L. Kuntz, Y. Zhou, Finite element analysis of effects of soft zones on formability of laser welded advanced high strength steels, Sci. Technol. Weld. Join. 14 (2009) 52–61.

[8] J. Rojek, M. Hyrcza-Michalska, A. Bokota, W. Piekarska, Determination of mechanical properties of the weld zone in tailor-welded blanks, Arch. Civ. Mech. Eng. 12 (2012) 156–162.

[9] U.S. Dixit, S.N. Joshi, J.P. Davim, Application of Lasers in Manufacturing: Select Papers from AIMTDR 2016, Springer, 2019.

[10] Q.S. Liu, S.M. Mahdavian, D. Aswin, S. Ding, Experimental study of temperature and clamping force during Nd: YAG laser butt welding, Opt. Laser Technol. 41 (2009) 794–799.

[11] B.S. Yilbas, A.F.M. Arif, B.J.A. Aleem, Laser welding of low carbon steel and thermal stress analysis, Opt. Laser Technol. 42 (2010) 760–768.

[12] R.S. Sharma, P. Molian, Weldability of advanced high strength steels using an Yb: YAG disk laser, J. Mater. Process. Technol. 211 (2011) 1888–1897.

[13] X. Xue, A.B. Pereira, J. Amorim, J. Liao, Effects of pulsed Nd: YAG laser welding parameters on penetration and microstructure characterization of a DP1000 steel butt joint, Metals (Basel). 7 (2017) 292.

[14] Z. Wang, J.P. Oliveira, Z. Zeng, X. Bu, B. Peng, X. Shao, Laser beam oscillating welding of 5A06 aluminum alloys: Microstructure, porosity and mechanical properties, Opt. Laser Technol. 111 (2019) 58–65.

[15] E. Assunção, L. Quintino, R. Miranda, Comparative study of laser welding in tailor blanks for the automotive industry, Int. J. Adv. Manuf. Technol. 49 (2010) 123–131.

[16] Q. Jia, W. Guo, W. Li, P. Peng, Y. Zhu, G. Zou, Y. Peng, Z. Tian, Experimental and numerical study on local mechanical properties and failure analysis of laser welded DP980 steels, Mater. Sci. Eng. A. 680 (2017) 378–387.

[17] U. Reisgen, M. Schleser, O. Mokrov, E. Ahmed, Shielding gas influences on laser weldability of tailored blanks of advanced automotive steels, Appl. Surf. Sci. 257 (2010)

1401–1406.

[18] M. Safari, M. Farzin, Experimental and numerical investigation of laser bending of tailor machined blanks, Opt. Laser Technol. 48 (2013) 513–522.

[19] M. Safari, M. Farzin, H. Mostaan, A novel method for laser forming of two-step bending of a dome shaped part, Iran. J. Mater. Form. 4 (2017) 1–14.

[20] M. Safari, M. Farzin, Experimental investigation of laser forming of a saddle shape with spiral irradiating scheme, Opt. Laser Technol. 66 (2015) 146–150.

[21] V.V.N.S. Suresh, S.P. Regalla, A.K. Gupta, Combined effect of thickness ratio and selective heating on weld line movement in stamped tailor-welded blanks, Mater. Manuf. Process. 32 (2017) 1363–1367.

[22] M.H. Asadian-Ardakani, M.R. Morovvati, M.J. Mirnia, B.M. Dariani, Theoretical and experimental investigation of deep drawing of tailor-welded IF steel blanks with non-uniform blank holder forces, Proc. Inst. Mech. Eng. Part B J. Eng. Manuf. 231 (2017) 286–300.

[23] S.K. Panda, N. Sreenivasan, M.L. Kuntz, Y. Zhou, Numerical simulations and experimental results of tensile test behavior of laser butt welded DP980 steels, J. Eng. Mater. Technol. 130 (2008) 41003.

[24] R.S. Korouyeh, H.M. Naeini, M.J. Torkamany, G. Liaghat, Experimental and theoretical investigation of thickness ratio effect on the formability of tailor welded blank, Opt. Laser Technol. 51 (2013) 24–31.

[25] T. Mennecart, A. Güner, N. Ben Khalifa, M. Hosseini, others, Deep Drawing of High-Strength Tailored Blanks by Using Tailored Tools, Materials (Basel). 9 (2016) 77.

[26] A.A. Zadpoor, J. Sinke, R. Benedictus, Elastoplastic deformation of dissimilar-alloy adhesively-bonded tailor-made blanks, Mater. Des. 31 (2010) 4611–4620. doi:https://doi.org/10.4028/www.scientific.net/KEM.344.373.

[27] H. Gong, S. Wang, P. Knysh, Y.P. Korkolis, Experimental investigation of the mechanical response of laser-welded dissimilar blanks from advanced-and ultra-high-strength steels, Mater. Des. 90 (2016) 1115–1123.

[28] M. Kardan, A. Parvizi, A. Askari, Influence of process parameters on residual stresses in deep-drawing process with FEM and experimental evaluations, J. Brazilian Soc. Mech. Sci. Eng. 40 (2018) 157.

[29] C.A. Secondary, C. Author, M. Kardan, A. Parvizi, A. Askari, M. Kardan, Journal of the Brazilian Society of Mechanical Sciences and Engineering Influence of Process Parameters on Residual Stresses in Deep Drawing Process with FEM and Experimental evaluations, (n.d.).

[30] R. Padmanabhan, M.C. Oliveira, H. Laurent, J.L. Alves, L.F. Menezes, Study on springback in deep drawn tailor welded blanks, Int. J. Mater. Form. 2 (2009) 829.

[31] R.S. Korouyeh, H.M. Naeini, M.J. Torkamany, J. Sabaghzadee, Effect of Laser Welding Parameters on Forming Behavior of Tailor Welded Blanks, in: Adv. Mater. Res., 2012: pp. 406–411.

[32] D. Rahmatabadi, M. Tayyebi, R. Hashemi, G. Faraji, Microstructure and mechanical properties of Al/Cu/Mg laminated composite sheets produced by the ARB proces, Int. J. Miner. Metall. Mater. 25 (2018) 564–572.

[33] D. Rahmatabadi, R. Hashemi, Experimental evaluation of forming limit diagram and mechanical properties of nano/ultra-fine grained aluminum strips fabricated by accumulative roll bonding, Int. J. Mater. Res. 108 (2017) 1036–1044.

[34] D. Rahmatabadi, M. Tayyebi, A. Sheikhi, R. Hashemi, Fracture toughness investigation of Al1050/Cu/MgAZ31ZB multi-layered composite produced by accumulative roll bonding process, Mater. Sci. Eng. A. 734 (2018) 427–436.

[35] J. Joudaki, others, Ovality and Bow Defect of Pre-punched Sheets in Roll Forming of Trapezoidal Sections, Int. J. Eng. 31 (2018) 1123–1128.

[36] F. Xiong, D. Wang, S. Chen, Q. Gao, S. Tian, Multi-objective lightweight and crashworthiness optimization for the side structure of an automobile body, Struct. Multidiscip. Optim. (2018) 1–21.

[37] D. Rahmatabadi, M. Pahlavani, A. Bayati, R. Hashemi, J. Marzbanrad, Evaluation of fracture toughness and rupture energy absorption capacity of as-rolled LZ71 and LZ91 Mg alloy sheet, Mater. Res. Express. 6 (2018) 36517.

[38] G. Sun, D. Tan, X. Lv, X. Yan, Q. Li, X. Huang, Multi-objective topology optimization of a vehicle door using multiple material tailor-welded blank (TWB) technology, Adv. Eng. Softw. 124 (2018) 1–9.

[39] M. Safari, J. Joudaki, Prediction of bending angle for laser forming of tailor machined blanks by neural network, Iran J Mater Form. 5 (2018) 47–57.

[40] A.T. Dhumal, R. Ganesh Narayanan, G. Saravana Kumar, Simulation based expert system to predict the deep drawing behaviour of tailor welded blanks, Int. J. Model. Identif. Control. 15 (2012) 164–172.

[41] S.M. Hamidinejad, M.H. Hasanniya, N. Salari, E. Valizadeh, CO 2 laser welding of interstitial free galvanized steel sheets used in tailor welded blanks, Int. J. Adv. Manuf. Technol. 64 (2013) 195–206.

[42] U. Reisgen, M. Schleser, O. Mokrov, E. Ahmed, Optimization of laser welding of DP/TRIP steel sheets using statistical approach, Opt. Laser Technol. 44 (2012) 255–262.

[43] J. Sun, J. Hensel, J. Klassen, T. Nitschke-Pagel, K. Dilger, Solid-state phase transformation and strain hardening on the residual stresses in S355 steel weldments, J. Mater. Process. Technol. 265 (2019) 173–184.

[44] A. Standard, E8," Standard Test Methods for Tension Testing of Metallic Materials,

Annu. B. ASTM Stand. 3 (2004) 57–72.

[45] M. Moradi, E. Golchin, Investigation on the effects of process parameters on laser percussion drilling using finite element methodology; statistical modelling and optimization, Lat. Am. J. Solids Struct. 14 (2017) 464–484. doi:10.1590/1679-78253247.

[46] J. Akai, TTT diagram of serpentine and saponite, and estimation of metamorphic heating degree of Antarctic carbonaceous chondrites, Antarct. Meteor. Res. 5 (1992) 120.

[47] A. Behzadi, E. Gholamian, P. Ahmadi, A. Habibollahzade, Energy , Exergy and Exergoeconomic ( 3E ) Analyses and multi-objective optimization of a solar and geothermal based integrated Energy System Energy , exergy and exergoeconomic ( 3E ) analyses and multi-objective optimization of a solar and geothermal base, Appl. Therm. Eng. 143 (2018) 1011–1022. doi:10.1016/j.applthermaleng.2018.08.034.

[48] C.P. Singh, G. Agnihotri, Study of deep drawing process parameters: a review, Int. J. Sci. Res. Publ. 5 (2015) 1–15.